Solar Physics (2021) 296:129
https://doi.org/10.1007/s11207-021-01875-5

About the Altitude Profile of the Atmospheric Cut-Off of Cosmic Rays: New Revised Assessment

Alexander Mishev[1,2] · **Stepan Poluianov**[1,2,3]

Received: 23 March 2021 / Accepted: 30 July 2021 / Published online: 25 August 2021

Abstract
Cosmic rays, high-energy subatomic particles of extraterrestrial origin, are systematically measured by space-borne and ground-based instruments. A specific interest is paid to high-energy ions accelerated during solar eruptions, so-called solar energetic particles. In order to build a comprehensive picture of their nature, it is important to fill the gap and inter-calibrate ground-based and space-borne instruments. Here, we focus on ground-based detectors, specifically neutron monitors, which form a global network and provide continuous recording of cosmic ray intensity and its variability, used also to register relativistic solar energetic particles. The count rate of each neutron monitor is determined by the geomagnetic and atmospheric cut-offs, both being functions of the location. Here, on the basis of Monte Carlo simulations with the PLANETOCOSMICS code and by the employment of a new verified neutron monitor yield function, we assessed the atmospheric cut-off as a function of the altitude, as well as for specific stations located in the polar region. The assessed in this study altitude profile of the atmospheric cut-off for primary cosmic rays builds the basis for the joint analysis of strong solar proton events with different instruments and allows one to clarify recent definitions and related discussions about the new sub-class of events, so-called sub-ground-level enhancements (sub-GLEs).

Keywords Cosmic rays · Solar energetic particles · Monte Carlo · Extensive air shower · Atmospheric cut-off · Neutron monitor

1. Introduction

The Earth is permanently bombarded by high-energy subatomic particles of extraterrestrial origin known as cosmic rays (CRs), viz. mostly protons, α-particles, and small amounts of heavier nuclei. Primary CRs are distributed in a wide energy range from about 10^6 eV

✉ S. Poluianov
stepan.poluianov@oulu.fi

A. Mishev
alexander.mishev@oulu.fi

1 Sodankylä Geophysical Observatory, University of Oulu, Oulu, Finland

2 Space Physics and Astronomy Research Unit, University of Oulu, Oulu, Finland

3 St. Petersburg State University, St. Petersburg, Russian Federation

nucleon^{-1} to extreme $\approx 10^{21}$ eV nucleon^{-1}. This energy distribution can be roughly approximated with a power-law spectrum (Beatty, Matthews, and Wakely, 2018). Nowadays, it is argued that the bulk of galactic cosmic rays (GCRs) originate from the Galaxy, following violent processes such as supernova explosions. A sporadic source of high-energy particles impinging the Earth's atmosphere is the Sun, viz. particles result from solar eruptive processes on it such as solar flares and coronal mass ejections. Hence, solar ions are accelerated to high energies and become solar energetic particles (SEPs) with energies usually of the order of tens of MeV nucleon^{-1}, rarely exceeding 100 MeV nucleon^{-1}, and in some cases reaching more than a few GeV nucleon^{-1} (e.g. Reames, 1999; Cliver, Kahler, and Reames, 2004; Desai and Giacalone, 2016).

When a high-energy primary CR particle enters the Earth's atmosphere, it interacts with an atmospheric constituent(s) and may produce new, i.e., secondary particle(s). Those secondary CRs also collide with the atmospheric constituents, in turn producing other secondaries, if their energy is above a certain threshold. In such a way, consecutive collisions add a large number of particles and form a cascade. As a result, a complicated nuclear-electromagnetic-mesonic air shower is developed in the atmosphere (Dorman, 2004; Grieder, 2010, and the references therein). The amount of the secondary particles increases until it reaches a maximum with its altitude being a function of the initial energy and the type of the primary particle. The depth of the maximum in the atmosphere depends also on the angle of incidence. It is about 400 – 500 g cm^{-2} or nearly 5 – 6 km of altitude above sea level for particles with energies in the "knee" region ($\approx 4 \cdot 10^{15}$ eV nucleon^{-1}) (for details see Engel, Heck, and Pierog, 2011; Grieder, 2010). After reaching its maximum, the cascade rapidly attenuates, so that the intensity of secondary electromagnetic and nucleonic particles exponentially decreases approaching sea level. Naturally, a primary particle with higher energy produces a greater amount of secondaries, and therefore, it has higher probability to be observed at ground comparing to a less energetic one. This effect can be represented by the atmospheric threshold (cut-off) energy (see e.g. Dorman, 2004). Primary CR particles with energies above the cut-off value can be registered by ground-based instrument(s), while insufficiently energetic ones have barely null detection probability.

Cosmic rays are systematically registered by space- and balloon-borne instruments as well as ground- and underground-based devices. Here, we focus on ground-based detectors, specifically neutron monitors (NMs). The NMs are the basis of a global network, which provides continuous recording of cosmic ray intensity and its variability since the mid-1950s (Simpson, Fonger, and Treiman, 1953; Hatton, 1971; Stoker, Dorman, and Clem, 2000; Mavromichalaki et al., 2011; Papaioannou et al., 2014). Those instruments are designed for registration of the secondary nucleonic component of a CR shower, details are given in Section 2. Besides, NM can register strong SEP events seen as so-called ground-level enhancements (GLEs) of the count rate over the galactic CR background (e.g., Shea and Smart, 1982; Dorman, 2004; Aschwanden, 2012; Poluianov et al., 2017). In fact, the global NM network provides key information for studies of GLEs, specifically on the high-energy part of their spectra (e.g., Mishev and Usoskin, 2020).

The count rate of each NM, aside from its instrumental efficiency, is determined by the geomagnetic and atmospheric cut-offs, both being functions of the location. The geomagnetic cut-off is due to the geomagnetic field shielding of the Earth from incoming CR charged particles (e.g., Dorman, 2009; Smart and Shea, 2009, and the references therein). This protection is maximal near to the geomagnetic equator (cut-off rigidity of about 17 GV) and marginal nearly 0 GV in the polar region (e.g., Smart and Shea, 2009). Accordingly, the atmospheric cut-off, as explained above, is determined by the thickness of air mass above the instrument usually expressed in g cm^{-2}. While the geomagnetic cut-off governs the NM

Table 1 Selected neutron monitors in the polar and sub-polar regions. Columns represent the station name, location, geomagnetic cut-off rigidity, altitude above sea level and type of the monitor. The table includes several high-altitude polar monitors and a new station (SUMT) proposed to extend the network.

Station	Latitude [deg]	Longitude [deg]	$P_{\mathrm{gm.cut}}$ [GV]	Altitude [m]	Type
Calgary (CALG)	51.08	245.87	1.08	1128	12NM64
Dome C (DOMC)	−75.06	123.20	0.01	3233	standard mini
Dome C (DOMB)	−75.06	123.20	0.01	3233	bare mini
Oulu (OULU)	65.05	25.47	0.69	15	9NM64
Sanae (SNA8)	−71.67	357.15	0.56	856	4NM80
South Pole (SOPO)	−90.00	0.0	0.09	2820	3NM64
South Pole (SOPB)	−90.00	0.0	0.09	2820	bare 6NM64
Terre Adelie (TERA)	−66.67	140.02	0.02	45	9NM64
Vostok (VSTK)	−78.47	106.87	0.01	3488	6NM64
Summit (SUMT)	72.34	321.73	0.01	3126	–

counting rate for the bulk of the stations, in the polar region, where the geomagnetic shielding is marginal, the atmospheric cut-off plays a major role. This is specifically important for the registration and study of SEPs. High-altitude polar stations (e.g., South Pole, Dome C, Vostok) possess notably lower atmospheric cut-offs than sea-level polar NMs (several such NMs are shown in Table 1 as examples). Therefore, high-altitude polar NMs are considerably more sensitive to SEPs, which allows one to register a recently introduced sub-class of events so-called sub-GLEs (for details see Poluianov et al., 2017). A systematic study of such events can provide the basis to fill the gap between space-borne and ground-based measurements of strong SEPs (e.g., Mishev, Poluianov, and Usoskin, 2017).

So far, the atmospheric cut-off was estimated mainly at the sea level by, e.g., latitude surveys, when NMs, usually onboard ships, scan a range of magnetic latitudes, so that the NM counting rate can be measured as a function of the geomagnetic cut-off rigidity (for details see e.g., Dorman et al., 2000; Villoresi et al., 2000; Dorman et al., 2008; Nuntiyakul et al., 2014). One can see that while the NM count rate increases with the diminishing geomagnetic cut-off in low and mid-latitudes, in the polar region, where the geomagnetic cut-off rigidity is about 1 GV or below, the NM count rate reaches a plateau (see Figures 2–4 and 5–7 in Villoresi et al., 2000; Nuntiyakul et al., 2014, respectively). This is due to the fact that in the polar region, the geomagnetic cut-off is lower than the atmospheric one, therefore the atmospheric shielding is more important. Thus, the atmospheric cut-off can be roughly estimated as about 1 GV, which corresponds to 433 MeV nucleon^{-1} for CR protons (Dorman, 2004; Grieder, 2010). Yet, this experimental assessment is applicable only for sea level detectors, while the atmospheric cut-off as a function of the altitude is poorly studied.

Here, we quantitatively assessed the atmospheric cut-off energy for cosmic-ray protons at different altitudes. We employed Monte Carlo simulations of atmospheric cascades and a recent verified NM yield function. We estimated both: (a) the physical atmospheric cut-off, i.e., the minimum energy of primary CR necessary to produce at least one secondary particle at a given altitude (observation level); (b) the instrumental cut-off, which is related to a particular instrument, namely NM64 at a given altitude, i.e. explicitly considering the registration efficiency of a specific device. We intentionally focused on cosmic-ray protons leaving α-particles and heavier species out of scope because their contribution to the total amount of SEPs is minor (see, e.g., Desai and Giacalone, 2016; Reames, 2019a,b)

This work follows a recent publication, where the definitions of GLE and sub-GLEs were revised (Poluianov et al., 2017) and is motivated by an active discussion related to registration and analysis of strong SEPs by ground-based and space-borne instruments (for details see Mishev, Poluianov, and Usoskin, 2017; Raukunen et al., 2018). It answers the question on the minimal energy of SEPs needed to get the event registered by neutron monitors at different altitudes in the polar regions.

2. Assessment of the Atmospheric Cut-Off Energy from Atmospheric Cascade Simulations

Recently, essential progress of Monte Carlo simulations of CR propagation in the atmosphere was achieved, based mostly on increased computation abilities and new data from hadron accelerators (e.g. Engel, Heck, and Pierog, 2011, and the references therein). A good example is the GEANT4 (Agostinelli et al., 2003) based PLANETOCOSMICS (Desorgher et al., 2005) code for simulations of interactions of cosmic rays with planetary atmospheres. It represents a tool for detailed studies of the evolution of CR-induced cascade, here employed specifically for the Earth atmosphere. The tool simulates interactions and decays of various nuclei, hadrons, mesons, electrons, and photons in the atmosphere up to high and very-high energies. The produced in interactions secondary particles are tracked through the atmosphere until they undergo reactions with air nuclei or decay. The result of the simulations is detailed information about the flux, spectrum, energy deposit, angle distribution of particles at given selected altitude(s) above sea level. The results from the atmospheric cascade simulations induced by primary CRs are in good agreement with experimental data, specifically the secondary neutron flux at different depths (e.g. Goldhagen, Clem, and Wilson, 2003, 2004; Pioch et al., 2011; Mishev, 2016; Woolf et al., 2019). This is particularly important for the estimation of the threshold energy of a primary CR particle to produce secondary particles at given altitude (depth) in the atmosphere.

In the energy range below one GeV nucleon^{-1}, individual contributions of secondary components in the CR-induced cascade at the ground level are dominated by neutrons because of the threshold energy required for the production of secondary leptons and mesons, and specifics of shower development (see Clem and Dorman, 2000; Engel, Heck, and Pierog, 2011, and the references therein for details).

Hence, we simulated CR-induced cascades due to primary protons around the energy range where previous studies reported an atmospheric cut-off of about 1 GV in rigidity or 433 MeV nucleon^{-1} in energy (Dorman, 2004; Grieder, 2010). We simulated cascades with isotropic and vertical incidence in the energy range 200 – 500 MeV nucleon^{-1} employing an updated version of the PLANETOCOSMICS code with the GEANT4 physics list QGSP_BIC_HP (the Quark-Gluon String model for high-energy interactions; Binary Cascade model; High-Precision neutron libraries) and a spherical atmospheric model NRLMSISE-00 (Picone et al., 2002). We considered isotropic and vertical incidence of particles because they determine the two extreme cases of the possible anisotropy of SEPs entering the atmosphere. The total amount of secondary particles, specifically neutrons, at several selected depths ranging from 600 g cm^{-2} (4.5 km of altitude) to 1033 g cm^{-2} (sea level) was derived. We built a distribution of the total amount of secondary particles vs. the energy of the primary, for several depths in the atmosphere. For example, the distribution of secondary CRs at sea level is presented in Figure 1A, and at 650 g cm^{-2} in Figure 1B, respectively. Note that the depth of 650 g cm^{-2} approximately corresponds to the highest

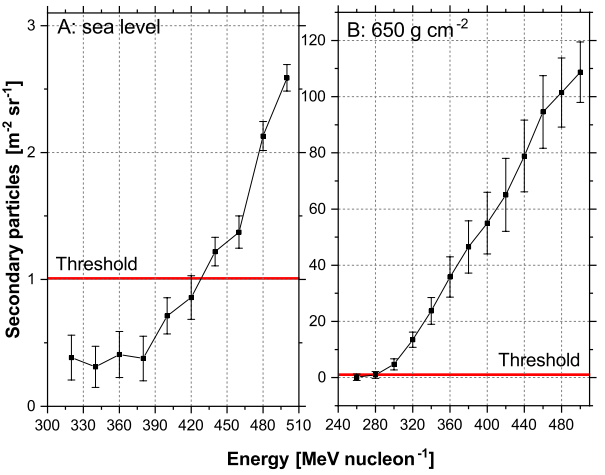

Figure 1 Secondary particles as a function of the energy for isotropic CRs. Panel A corresponds to sea level (1033 g cm^{-2} of the atmospheric depth), while panel B corresponds to 650 g cm^{-2}.

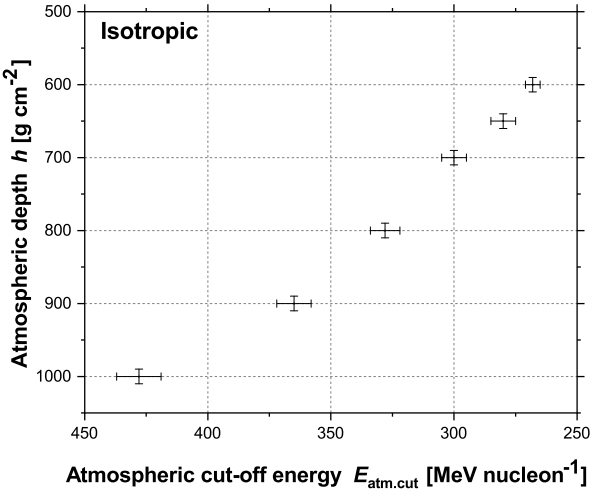

Figure 2 Atmospheric cut-off energies for CRs with isotropic incidence at selected depths in the atmosphere.

altitude with nearly null rigidity cut-off CR stations, namely DOMC/DOMB and VSTK; see Poluianov et al. (2015) and Table 1 for details.

The derived distribution represents the total amount of secondaries (normalized per unit primary particle flux) impinging the unit area on top of the atmosphere, at a selected depth, as a function of the primary particle energy. We assume one secondary particle reaching the selected depth as the threshold value. Therefore, the atmospheric cut-off is determined as the minimum energy of a primary CR proton necessary to induce a such cascade, that at least one secondary particle (in average) reaches the given atmospheric depth. Hence, we estimated the atmospheric cut-off at sea level to about 428 ± 9 MeV nucleon^{-1}, and 282 ± 5 MeV nucleon^{-1} at 650 g cm^{-2}, respectively. The altitude dependence of the atmospheric cut-off for protons with isotropic incidence is presented in Figure 2, the details are given in Table 2.

Accordingly, similar computations were performed for primary CR protons with vertical incidence, i.e., particles traversing minimal amount of air mass, which have a naturally

Table 2 Atmospheric cut-off energies computed with Monte Carlo simulations for CRs with isotropic and vertical incidence at selected depths in the atmosphere.

Depth [g cm^{-2}]	Atmospheric cut-off energy [MeV]	
	isotrop. CR	vertical CR
600	268 ± 3	186 ± 3
650	282 ± 5	203 ± 4
700	301 ± 5	225 ± 4
800	328 ± 6	268 ± 5
900	365 ± 7	302 ± 7
1000	408 ± 8	342 ± 8
1033	428 ± 9	357 ± 8

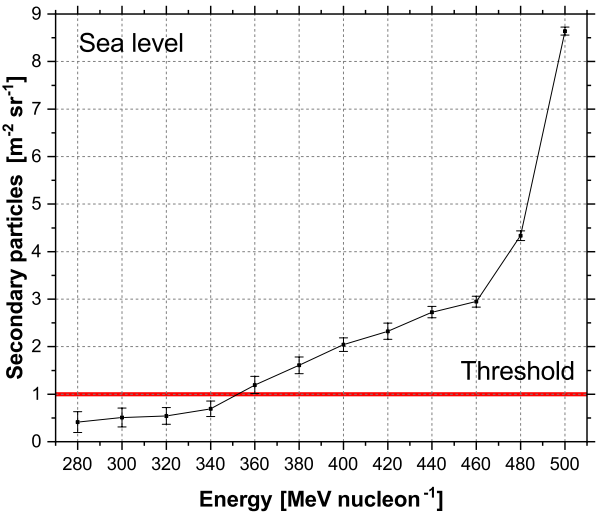

Figure 3 Secondary particles as a function of the energy for vertically arriving CRs at sea level (1033 g cm^{-2} of the atmospheric depth).

lower cut-off. Note, in most cases of GLE analysis, SEPs are usually assumed with only vertical incidence (Bütikofer et al., 2009; Plainaki et al., 2014; Mishev et al., 2021). It is actually the case also for sub-GLEs. The distribution of secondary particles at sea level as a function of the energy of the primary CR proton with vertical incidence is given in Figure 3. The altitude dependence of the atmospheric cut-off for protons with vertical incidence is presented in Figure 4, the details are given in Table 2. Detailed information about the estimated atmospheric cut-off for primary CR protons with isotropic and vertical incidence at selected depths is summarized in Table 2. The derived atmospheric cut-off for particles with an isotropic incidence at sea level is comparable with previous reports as well as with some recent estimations (e.g Dorman, 2004; Grieder, 2010; Raukunen et al., 2018). However, naturally the Monte Carlo estimation of the atmospheric cut-off results in slightly lower values, because the detector efficiency is not considered here.

Therefore in addition to the physical cut-off, it is necessary to perform similar estimations for a given type of detector, namely neutron monitor. This is particularly important for justification and clarification of the current definition of sub-GLEs, and GLEs concerning the energy of registered SEPs (for details see Poluianov et al., 2017; Raukunen et al., 2018).

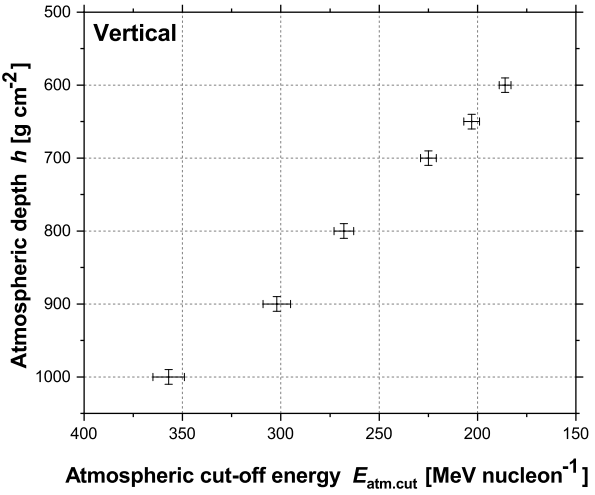

Figure 4 Atmospheric cut-off energies for CRs with vertical incidence at selected depths in the atmosphere.

3. Assessment of the Atmospheric Cut-Off Energy with the NM Yield Function

In the previous section, the atmospheric cut-off was estimated from the point of view of an ideal detector, i.e., a detector, which registers secondary nucleonic particles with 100% efficiency. However, real instruments possess limited registration ability.

Here, we considered a standard instrument for monitoring cosmic rays and their variations, namely a neutron monitor. NM count rate records allow one to study CR flux variations at the top of the Earth's atmosphere at different time scales (e.g. diurnal, 11-year sunspot cycle, 22-year solar magnetic cycle), as well as short-term transients such as Forbush decreases and anisotropic cosmic ray enhancements (for details see Moraal, 1976; Debrunner et al., 1988; Lockwood, Debrunner, and Flueckiger, 1990; Gil et al., 2018). Neutron monitors are in practice the main detectors for continuous recording of CR intensity variations (e.g. Moraal, 1976; Debrunner et al., 1988; Gil et al., 2015; Kudela, 2016). In addition, registration of GLEs and sub-GLEs with NMs provides key information for analysis of the spectral and angular characteristics over the whole time span of those events (e.g. Shea and Smart, 1982; Cramp et al., 1997; Bombardieri et al., 2006; Vashenyuk et al., 2006; Mishev, Kocharov, and Usoskin, 2014; Mishev et al., 2018).

NM is a ground-based detector aiming the registration of secondary particles, mostly neutrons, but also protons and a small amount of muons, produced in a cosmic-ray cascade (Simpson, 1957; Clem and Dorman, 2000). The instrument consists of one or several proportional counters sensitive to thermal neutrons and filled with enriched to ^{10}B boron-trifluoride or ^{3}He gas, surrounded by a moderator, usually paraffin wax or polyethylene, a lead "producer" and an outer reflector made of the same material as the moderator (for details see Clem and Dorman, 2000; Simpson, 2000; Bütikofer, 2018, and the references therein). It was introduced as a continuous recorder of the CR intensity during the International Geophysical Year (IGY) 1957–1958 (Simpson, 1957). In 1964, the design was optimized. The improved instrument is known as the supermonitor or NM64 (see Hatton and Carmichael, 1964; Carmichael, 1968; Simpson, 2000; Stoker, Dorman, and Clem, 2000, and the references therein for details). Nowadays, the NM64 supermonitors are the main detectors in the global NM network, though other designs are also in use (e.g. Mishev and Usoskin, 2020).

For the computation of the instrumental atmospheric cut-off, we employed the NM yield function, which represents the response of the NM to the unit flux of CRs with given energy impinging the top of the atmosphere (e.g. Clem and Dorman, 2000; Flückiger et al., 2008; Mishev, Usoskin, and Kovaltsov, 2013). The yield function incorporates the full complexity of the atmospheric cascade development, interaction(s) of the secondary particles with the detector, taking into account the registration efficiency itself. Here, we considered the standard 6NM64 detector for the computations.

Using the yield function, the NM count rate $N(h)$ [counts s^{-1}] can be computed as

$$N(h) = \sum_{i=p,\alpha} \int_{P_{\mathrm{gm.cut}}}^{\infty} Y_i(P,h) J_i(P)\, dP, \tag{1}$$

where $Y_i(P,h)$ is the yield function for incident CRs of ith type (protons, α-particles and heavier ions, which are scaled to and effectively accounted as α-particles (e.g. Mishev, Usoskin, and Kovaltsov, 2013)) in units of [counts m^2 sr], $J_i(P)$ is the differential flux of GCRs of ith type in [s m^2 sr GV/nucleon]$^{-1}$, h is the atmospheric depth of the instrument in [g cm^{-2}], P is the CR particle's rigidity [GV], $P_{\mathrm{gm.cut}}$ is the local geomagnetic cut-off rigidity of the instrument in [GV] (Cooke et al., 1991; Smart et al., 2006).

The NM yield function is continuous and only asymptotically approaches zero, i.e., there is not apparent cut-off (see Figure 1 in Mishev et al., 2020). Therefore, it is necessary to exclude the geomagnetic effects and elaborate a realistic signal-to-noise ratio in an attempt to assess the atmospheric cut-off.

Here, we considered a NM located in the polar region with the geomagnetic cut-off rigidity $P_{gm.cut} = 0$ GV and effectively excluded the influence of the geomagnetic field. Equation 1 for ith type of CR particles can be rewritten as an integral over energy E

$$N_i(h) = \int_0^{\infty} Y_i(E,h) J_i(E)\, dE, \tag{2}$$

where the differential flux $J_i(E)$ is in [s m^2 sr GeV/nucleon]$^{-1}$.

Note that the energy–rigidity relation for a particle of type i is given by

$$E(P) = \sqrt{\left(\frac{Z_i}{A_i}\right)^2 P^2 + E_0^2} - E_0, \tag{3}$$

where $E_0 = 0.938$ GeV is the proton's rest energy, A and Z are the mass and charge numbers, respectively.

In turn, equation (2) can be split to a sum of two integrals:

$$N_i(h) = \underbrace{\int_{E_c}^{\infty} Y_i(E,h) J_i(E)\, dE}_{I_{1,i}(h,E_c)} + \underbrace{\int_0^{E_c} Y_i(E,h) J_i(E)\, dE}_{I_{2,i}(h,E_c)}, \tag{4}$$

where E_c is the integration parameter, the details are given below.

Here, we assumed that the first term $I_{1,i}(h, E_c)$ accounts the major fraction of counts, while the second term $I_{2,i}(h, E_c)$ accounts the remainder due to low-energy particles, that is, the contribution from zero to E_c.

Henceforth, we focus on primary protons ($i = p$), whilst the contribution of α-particles and heavier ions is insignificant in the particular application to the solar particle events, as

discussed above. Naturally, the atmospheric cut-off energy $E_{\mathrm{atm.cut}}$ is defined as the maximum energy E_{c}, where the contribution of $I_{2,p}(h, E_{\mathrm{c}})$ to the total count rate $N(h)$ is indistinguishable.

The contribution of the term $I_{2,p}(h, E_{\mathrm{c}})$ can be indistinguishable to the total count rate because of the random variability of the count rate $N(h)$ around certain mean value $\langle N(h)\rangle$ with the standard deviation $\sigma(h)$. The NM count rate reveals the Poisson distribution. Accordingly, its standard deviation is $\sigma(h) = \sqrt{\langle N(h)\rangle}$. The mean count rate $\langle N(h)\rangle$ can be computed using Equation 2. For these computations of the NM count rate at several depths in the atmosphere, we employed the newly computed NM yield function by Mishev et al. (2020). The new yield function is in very good agreement with the experimental latitude surveys and was recently validated by measurements (Gil et al., 2015; Nuntiyakul et al., 2018). Moreover, it was additionally verified using space-borne data (for details see Koldobskiy et al., 2019). The function is presented in tabular and parametrized forms for convenience.

Here, we considered galactic cosmic rays employing the force-field model (Gleeson and Axford, 1968), which is sufficiently accurate for the aims of this work (Usoskin et al., 2015). The differential energy CR spectrum $J_i(E)$ is expressed as

$$J_i(E) = J_{\mathrm{LIS},i}\left(E + \frac{Z_i}{A_i}\phi\right) \cdot \frac{E(E+2E_0)}{(E+\frac{Z_i}{A_i}\phi)(E+\frac{Z_i}{A_i}\phi+2E_0)}, \tag{5}$$

where $J_{\mathrm{LIS},i}$ is the differential flux of GCRs of ith type in the local interstellar medium [s m^2 sr GeV/nuc]$^{-1}$, E is the GCR kinetic energy [GeV nucleon^{-1}], ϕ is the potential [GV] representing the heliospheric modulation of GCRs. The local interstellar spectrum $J_{\mathrm{LIS},i}$ was taken according to Vos and Potgieter (2015) with the ratio of α-particle and heavier ion nuclei to protons as 0.353 (Koldobskiy et al., 2019).

We computed the integral normalized to the standard deviation $I_{2,p}(h, E_{\mathrm{c}})/\sigma(h)$ over a range of E_{c} (Equation 4, Figure 5). There is a threshold $T = I^{\mathrm{th}}_{2,p}(h)/\sigma(h)$, which is invariant to the total count rate $N(h)$, where the contribution of $I_{2,p}(h, E_{\mathrm{c}})$ becomes indistinguishable to the total count:

$$T = \frac{I^{\mathrm{th}}_{2,p}(h)}{\sigma(h)} = \mathrm{const.} \tag{6}$$

Therefore, the atmospheric cut-off energy $E_{\mathrm{atm.cut}}$ is a point, where $I_{2,p}(h, E_{\mathrm{c}})/\sigma(h)$ intersects T, as depicted in Figure 5. Note that the experimental latitude surveys, as discussed above, imply the atmospheric cut-off energy $E_{\mathrm{atm.cut}}$ of about 433 MeV nucleon^{-1} at sea level ($h = 1033$ g/cm^2) and T is constant, as depicted with horizontal dashed line in Figure 5.

The computations of $I_{2,p}(h, E_{\mathrm{c}})/\sigma(h)$ were performed for the mean modulation potential $\phi = 652$ MV (1951–2019, http://cosmicrays.oulu.fi/phi/phi.html, Usoskin et al. (2017)), as well as for $\phi = 300$ MV and $\phi = 1200$ MV, which correspond to low and high solar activity conditions, respectively. Thereby, the influence of cosmic ray modulation on atmospheric cut-off was estimated. Details for those computations are given in Table 3. One can see that the solar variability causes only marginal effect of about $\pm 1\%$ on the derived atmospheric cut-off.

The altitude profiles of the atmospheric cut-off energies obtained with the cascade simulations and with the verified NM yield function are presented in Figure 6. Naturally, a smooth, monotonic increase of the atmospheric cut-off from low depths towards sea level, is observed. As expected, the atmospheric cut-off computed specifically for NM is greater compared to that obtained from the atmospheric cascade simulations. As an example, it is

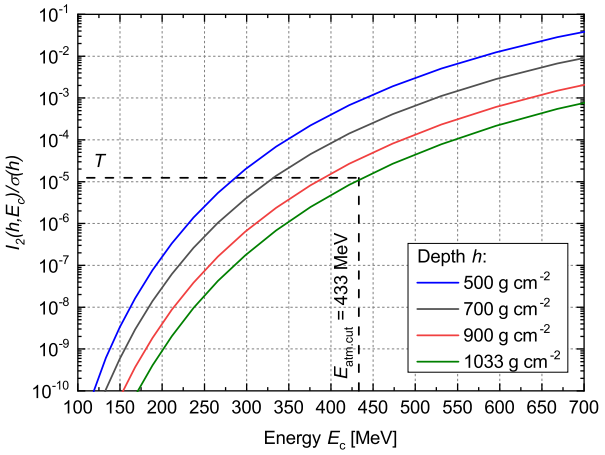

Figure 5 Remainder integral $I_{2,p}(h, E_c)/\sigma(h)$ (Equation 4) for different atmospheric depths h, as depicted in the legend. The horizontal dashed line indicates the estimated threshold T (Equation 6).

Table 3 Atmospheric cut-off energies at selected depths estimated with the NM yield function and computed for different heliospheric modulation potentials. The column $\phi = 652$ MV corresponds to the mean value of the potential for 1951 – 2019.

Depth [g cm^{-2}]	Atmospheric cut-off energy [MeV]		
	652 MV	300 MV	1200 MV
600	304.15	302.41	305.33
700	330.10	326.76	332.52
800	354.47	352.56	355.83
900	386.16	385.18	386.83
1000	424.18	423.86	424.40
1033	433.00	433.00	433.00

greater by 26 MeV (7%) at 800 g/cm^2 and by 36 MeV (12%) at 600 g/cm^2, respectively. This is due to specifics of the altitudinal profile of NM yield function leading to increase of the absolute standard deviation $\sigma(h)$ of the count rate as a function of the altitude, in spite of its reduction in relative units $\sigma(h)/\langle N(h)\rangle$, as well as intrinsic cascade fluctuations considered in shower simulations (for details see Engel, Heck, and Pierog, 2011; Mishev et al., 2020).

4. Discussion and Conclusions

During the last decades, SEPs have been extensively studied using space probes, such as GOES (Geo-stationary Operational Environmental Satellites). However, most of the space-borne experiments were/are focused on measurements in the low-energy range of solar ions, therefore possess apparent constraints for the precise study of the most energetic ones, e.g. leading to GLEs. Yet, SoHO/EPHIN (Solar-Heliospheric Observatory/Electron Proton and Helium Instrument) and GOES/HEPAD (High Energy Proton and Alpha Detector) have enhanced energy channels up to 500 MeV nucleon^{-1} and up to about 700 MeV nucleon^{-1}, respectively (for details see Kühl et al., 2017), as well as PAMELA (Payload for Antimatter

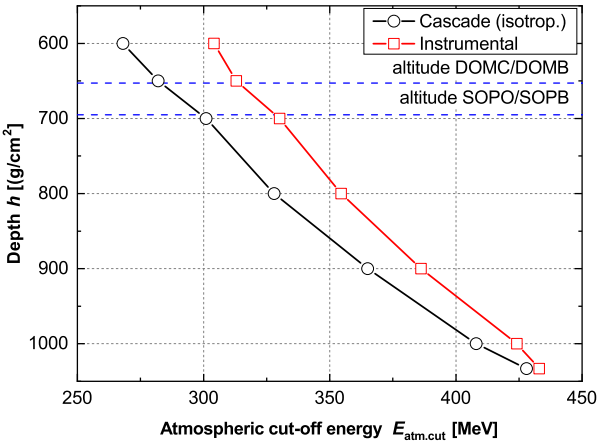

Figure 6 Comparison of the atmospheric cut-off energy values computed with the cascade simulations and NM yield function (the latter with $J_{\mathrm{LIS},i}$ according to Vos and Potgieter (2015), $\phi = 652$ MV, which is the mean for 1951–2019, Usoskin et al. (2017)). Blue horizontal dash lines correspond to the atmospheric depths of DOMC/DOMB and SOPO/SOPB NMs, respectively.

Matter Exploration and Light-nuclei Astrophysics) and AMS-02 (Alpha Magnetic Spectrometer) designed to measure directly more energetic particles (e.g., Adriani et al., 2016). Therefore, assessment of the atmospheric cut-off for a specific device such as NM, which is widely used for GLE studies, gives the basis to fill the gap and inter-calibrate the ground-based and space-borne instruments for SEP measurements.

Here, the most sensitive high-altitude polar NMs revealed the following atmospheric cut-off energies: 283 MeV (atmospheric cascade simulation) and 314 MeV (NM yield function employment) for DOMC/DOMB and 299 MeV (atmospheric cascade simulation) and 328 MeV (NM yield function employment) for SOPO/SOPB (Figure 6). One can see that the atmospheric cut-off assessed with cascade simulations is slightly lower than one estimated with the NM yield function. While the atmospheric cascade simulations are related to an ideal detector with 100% registration efficiency and reveal the physical signal, the more conservative approach for a specific detector, namely NM, is more realistic. This is particularly important for clarification of recent definitions and related discussions about sub-GLEs, a specific sub-class of SEPs, observed by SOPO/SOPB and DOMC/DOMB NM and at space, but not at sea-level instruments (Poluianov et al., 2017; Raukunen et al., 2018). We can conclude that the definitions of sub-GLE given by Raukunen et al. (2018) (based on the lower energy limit 300 MeV) and by Poluianov et al. (2017) (based on the simultaneous observation by SOPO and DOMC), are in very good agreement.

The assessed in this study atmospheric cut-off for primary CRs, specifically employed for SEPs, gives the basis for the joint analysis of GLEs, filling the gap between ground-based and space-borne instruments and the development of forefront methods for their studies.

Acknowledgements This work was supported by the Academy of Finland (projects 330064 QUASARE and 321882 ESPERA). It was motivated and benefited from discussions in the framework of the International Space Science Institute International Team 441: High EneRgy sOlar partICle Events Analysis (HEROIC). SP acknowledges support by the Russian Science Foundation (RSF project No. 20-67-46016).

Funding Note Open access funding provided by University of Oulu including Oulu University Hospital.

Declarations

Disclosure of Potential Conflicts of Interest The authors declare that they do not have conflicts of interest.

References

Adriani, O., Barbarino, G.C., Bazilevskaya, G.A., Bellotti, R., Boezio, M., et al.: 2016, Measurements of cosmic-ray hydrogen and helium isotopes with the PAMELA experiment. *Astrophys. J.* **818**, 68. DOI. ADS.

Agostinelli, S., Allison, J., Amako, K., et al.: 2003, Geant4—a simulation toolkit. *Nucl. Instrum. Methods Phys. Res., Sect. A, Accel. Spectrom. Detect. Assoc. Equip.* **506**, 250. DOI.

Aschwanden, M.J.: 2012, GeV particle acceleration in solar flares and Ground Level Enhancement (GLE) events. *Space Sci. Rev.* **171**, 3. DOI. ADS.

Beatty, J.J., Matthews, J., Wakely, S.P.: 2018, Cosmic rays. In: Tanabashi, M. et al. (ed.) *Review of Particle Physics*. DOI. Phys. Rev. D 98, 030001, 424.

Bombardieri, D.J., Duldig, M.L., Michael, K.J., Humble, J.E.: 2006, Relativistic proton production during the 2000 July 14 solar event: the case for multiple source mechanisms. *Astrophys. J.* **644**, 565. DOI. ADS.

Bütikofer, R.: 2018, In: Malandraki, O.E., Crosby, N.B. (eds.) *Ground-Based Measurements of Energetic Particles by Neutron Monitors* **444**, 95. DOI. ADS.

Bütikofer, R., Flückiger, E.O., Desorgher, L., Moser, M.R., Pirard, B.: 2009, The solar cosmic ray ground-level enhancements on 20 January 2005 and 13 December 2006. *Adv. Space Res.* **43**, 499. DOI. ADS.

Carmichael, H.: 1968, Cosmic rays (instruments). In: Minnis, C.M. (ed.) *Ann. IQSY* **1**, MIT Press, Cambridge, 178.

Clem, J.M., Dorman, L.I.: 2000, Neutron monitor response functions. *Space Sci. Rev.* **93**, 335. DOI. ADS.

Cliver, E.W., Kahler, S.W., Reames, D.V.: 2004, Coronal shocks and solar energetic proton events. *Astrophys. J.* **605**, 902. DOI. ADS.

Cooke, D.J., Humble, J.E., Shea, M.A., Smart, D.F., Lund, N., Rasmussen, I.L., Byrnak, B., Goret, P., Petrou, N.: 1991, On cosmic-ray cut-off terminology. *Nuovo Cimento C* **14**, 213. DOI. ADS.

Cramp, J.L., Duldig, M.L., Flückiger, E.O., Humble, J.E., Shea, M.A., Smart, D.F.: 1997, The October 22, 1989, solar cosmic ray enhancement: an analysis of the anisotropy and spectral characteristics. *J. Geophys. Res.* **102**, 24237. DOI. ADS.

Debrunner, H., Flueckiger, E., Graedel, H., Lockwood, J.A., McGuire, R.E.: 1988, Observations related to the acceleration, injection, and interplanetary propagation of energetic protons during the solar cosmic ray event on February 16, 1984. *J. Geophys. Res.* **93**, 7206. DOI. ADS.

Desai, M., Giacalone, J.: 2016, Large gradual solar energetic particle events. *Living Rev. Solar Phys.* **13**, 3. DOI.

Desorgher, L., Flückiger, E.O., Gurtner, M., Moser, M.R., Bütikofer, R.: 2005, Atmocosmics: a Geant 4 code for computing the interaction of cosmic rays with the Earth's atmosphere. *Int. J. Mod. Phys. A* **20**, 6802. DOI. ADS.

Dorman, L.: 2009, *Cosmic Rays in Magnetospheres of the Earth and Other Planets*, Springer, Dordrecht. DOI. 978-1-4020-9238-1. ADS.

Dorman, L.I.: 2004, *Cosmic Rays in the Earth's Atmosphere and Underground* **303**, Kluwer Academic Publishers, Dordrecht. DOI. 1-4020-2071-6. ADS.

Dorman, L.I., Villoresi, G., Iucci, N., Parisi, M., Tyasto, M.I., Danilova, O.A., Ptitsyna, N.G.: 2000, Cosmic ray survey to Antarctica and coupling functions for neutron component near solar minimum (1996 – 1997) 3. Geomagnetic effects and coupling functions. *J. Geophys. Res.* **105**, 21047. DOI. ADS.

Dorman, L.I., Danilova, O.A., Iucci, N., Parisi, M., Ptitsyna, N.G., Tyasto, M.I., Villoresi, G.: 2008, Effective non-vertical and apparent cutoff rigidities for a cosmic ray latitude survey from Antarctica to Italy in minimum of solar activity. *Adv. Space Res.* **42**, 510. DOI.

Engel, R., Heck, D., Pierog, T.: 2011, Extensive air showers and hadronic interactions at high energy. *Annu. Rev. Nucl. Part. Sci.* **61**, 467. DOI. ADS.

Flückiger, E.O., Moser, M.R., Pirard, B., Bütikofer, R., Desorgher, L.: 2008, A parameterized neutron monitor yield function for space weather applications. In: *International Cosmic Ray Conference*, *International Cosmic Ray Conference* **1**, 289. ADS.

Gil, A., Usoskin, I.G., Kovaltsov, G.A., Mishev, A.L., Corti, C., Bindi, V.: 2015, Can we properly model the neutron monitor count rate? *J. Geophys. Res.* **120**, 7172. DOI. ADS.
Gil, A., Kovaltsov, G.A., Mikhailov, V.V., Mishev, A., Poluianov, S., Usoskin, I.G.: 2018, An anisotropic cosmic-ray enhancement event on 07-June-2015: a possible origin. *Solar Phys.* **293**, 154. DOI. ADS.
Gleeson, J.J., Axford, W.I.: 1968, Solar modulation of galactic cosmic rays. *Astrophys. J.* **154**, 1011. DOI. ADS.
Goldhagen, P., Clem, J.M., Wilson, J.W.: 2003, Recent results from measurements of the energy spectrum of cosmic-ray induced neutrons aboard an er-2 airplane and on the ground. *Adv. Space Res.* **32**, 35. DOI.
Goldhagen, P., Clem, J.M., Wilson, J.W.: 2004, The energy spectrum of cosmic-ray induced neutrons measured on an airplane over a wide range of altitude and latitude. *Radiat. Prot. Dosim.* **110**, 387. DOI.
Grieder, P.K.F.: 2010, *Extensive Air Showers: High Energy Phenomena and Astrophysical Aspects – A Tutorial, Reference Manual and Data Book*, Springer, Berlin. DOI. ISBN 978-3540769408. ADS.
Hatton, C.: 1971, The neutron monitor. In: *Progress in Elementary Particle and Cosmic-ray Physics X*, North Holland Publishing Co., Amsterdam, 3. Chap. 1.
Hatton, C.J., Carmichael, H.: 1964, Experimental investigation of the NM-64 neutron monitor. *Can. J. Phys.* **42**, 2443. DOI. ADS.
Koldobskiy, S.A., Bindi, V., Corti, C., Kovaltsov, G.A., Usoskin, I.G.: 2019, Validation of the neutron monitor yield function using data from AMS-02 experiment 2011 – 2017. *J. Geophys. Res.* **124**, 2367. DOI.
Kudela, K.: 2016, On low energy cosmic rays and energetic particles near Earth. *Contrib. Astron. Obs. Skaln. Pleso* **46**, 15. ADS.
Kühl, P., Dresing, N., Heber, B., Klassen, A.: 2017, Solar energetic particle events with protons above 500 MeV between 1995 and 2015 measured with SOHO/EPHIN. *Solar Phys.* **292**, 10. DOI.
Lockwood, J.A., Debrunner, H., Flueckiger, E.O.: 1990, Indications for diffusive coronal shock acceleration of protons in selected solar cosmic ray events. *J. Geophys. Res.* **95**, 4187. DOI. ADS.
Mavromichalaki, H., Papaioannou, A., Plainaki, C., Sarlanis, C., Souvatzoglou, G., et al.: 2011, Applications and usage of the real-time Neutron Monitor Database. *Adv. Space Res.* **47**, 2210. DOI. ADS.
Mishev, A.L.: 2016, Contribution of cosmic ray particles to radiation environment at high mountain altitude: comparison of Monte Carlo simulations with experimental data. *J. Environ. Radioact.* **153**, 15. DOI.
Mishev, A., Usoskin, I.: 2020, Current status and possible extension of the global neutron monitor network. *J. Space Weather Space Clim.* **10**, 20020. DOI.
Mishev, A., Poluianov, S., Usoskin, S.: 2017, Assessment of spectral and angular characteristics of sub-gle events using the global neutron monitor network. *J. Space Weather Space Clim.* **7**, A28. DOI.
Mishev, A.L., Kocharov, L.G., Usoskin, I.G.: 2014, Analysis of the ground level enhancement on 17 May 2012 using data from the global neutron monitor network. *J. Geophys. Res.* **119**, 670. DOI. ADS.
Mishev, A.L., Usoskin, I.G., Kovaltsov, G.A.: 2013, Neutron monitor yield function: new improved computations. *J. Geophys. Res.* **118**, 2783. DOI. ADS.
Mishev, A.L., Koldobskiy, S.A., Kovaltsov, G.A., Gil, A., Usoskin, I.G.: 2020, Updated neutron-monitor yield function: bridging between in situ and ground-based cosmic ray measurements. *J. Geophys. Res.* **125**, e27433. DOI. ADS.
Mishev, A.L., Koldobskiy, S.A., Kocharov, L.G., Usoskin, I.G.: 2021, GLE # 67 event on 2 November 2003: an analysis of the spectral and anisotropy characteristics using verified yield function and detrended neutron monitor data. *Solar Phys.* **296**, 79. DOI. ADS.
Mishev, A., Usoskin, I., Raukunen, O., Paassilta, M., Valtonen, E., Kocharov, L., Vainio, R.: 2018, First analysis of Ground-Level Enhancement (GLE) 72 on 10 September 2017: spectral and anisotropy characteristics. *Solar Phys.* **293**, 136. DOI. ADS.
Moraal, H.: 1976, Observations of the eleven-year cosmic-ray modulation cycle. *Space Sci. Rev.* **19**, 845. DOI. ADS.
Nuntiyakul, W., Evenson, P., Ruffolo, D., Sáiz, A., Bieber, J.W., Clem, J., Pyle, R., Duldig, M.L., Humble, J.E.: 2014, Latitude survey investigation of galactic cosmic ray solar modulation during 1994 – 2007. *Astrophys. J.* **795**, 11. DOI. ADS.
Nuntiyakul, W., Sáiz, A., Ruffolo, D., Mangeard, P.-S., Evenson, P., Bieber, J.W., Clem, J., Pyle, R., Duldig, M.L., Humble, J.E.: 2018, Bare neutron counter and neutron monitor response to cosmic rays during a 1995 latitude survey. *J. Geophys. Res.* **123**, 7181. DOI.
Papaioannou, A., Souvatzoglou, G., Paschalis, P., Gerontidou, M., Mavromichalaki, H.: 2014, The first ground-level enhancement of solar cycle 24 on 17 May 2012 and its real-time detection. *Solar Phys.* **289**, 423. DOI.
Picone, J.M., Hedin, A.E., Drob, D.P., Aikin, A.C.: 2002, NRLMSISE-00 empirical model of the atmosphere: statistical comparisons and scientific issues. *J. Geophys. Res.* **107**, SIA 15. 1468. DOI.
Pioch, C., Mares, V., Vashenyuk, E.V., Balabin, Y.V., Rühm, W.: 2011, Measurement of cosmic ray neutrons with Bonner sphere spectrometer and neutron monitor at 79°n. *Nucl. Instrum. Methods Phys. Res., Sect. A, Accel. Spectrom. Detect. Assoc. Equip.* **626-627**, 51. DOI.

Plainaki, C., Mavromichalaki, H., Laurenza, M., Gerontidou, M., Kanellakopoulos, A., Storini, M.: 2014, The ground-level enhancement of 2012 May 17: derivation of solar proton event properties through the application of the NMBANGLE PPOLA model. *Astrophys. J.* **785**, 160. DOI.

Poluianov, S., Usoskin, I., Mishev, A., Moraal, H., Kruger, H., Casasanta, G., Traversi, R., Udisti, R.: 2015, Mini neutron monitors at Concordia research station, central Antarctica. *J. Astron. Space Sci.* **32**, 281. DOI. ADS.

Poluianov, S.V., Usoskin, I.G., Mishev, A.L., Shea, M.A., Smart, D.F.: 2017, GLE and sub-GLE redefinition in the light of high-altitude polar neutron monitors. *Solar Phys.* **292**, 176. DOI.

Raukunen, O., Vainio, R., Tylka, A.J., Dietrich, W.F., Jiggens, P., Heynderickx, D., Dierckxsens, M., Crosby, N., Ganse, U., Siipola, R.: 2018, Two solar proton fluence models based on ground level enhancement observations. *J. Space Weather Space Clim.* **8**, A04. DOI. ADS.

Reames, D.V.: 1999, Particle acceleration at the Sun and in the heliosphere. *Space Sci. Rev.* **90**, 413. DOI.

Reames, D.V.: 2019a, Hydrogen and the abundances of elements in gradual solar energetic-particle events. *Solar Phys.* **294**, 69. DOI. ADS.

Reames, D.V.: 2019b, Hydrogen and the abundances of elements in impulsive solar energetic-particle events. *Solar Phys.* **294**, 37. DOI. ADS.

Shea, M.A., Smart, D.F.: 1982, Possible evidence for a rigidity-dependent release of relativistic protons from the solar corona. *Space Sci. Rev.* **32**, 251. DOI. ADS.

Simpson, J.: 1957, Cosmic-radiation neutron intensity monitor. *Ann. Int. Geophys. Year* **4**, 351.

Simpson, J.: 2000, The cosmic ray nucleonic component: the invention and scientific uses of the neutron monitor. *Space Sci. Rev.* **93**, 11. DOI.

Simpson, J.A., Fonger, W., Treiman, S.B.: 1953, Cosmic radiation intensity-time variations and their origin. I. Neutron intensity variation method and meteorological factors. *Phys. Rev.* **90**, 934. DOI. ADS.

Smart, D.F., Shea, M.A.: 2009, Fifty years of progress in geomagnetic cutoff rigidity determinations. *Adv. Space Res.* **44**, 1107. DOI.

Smart, D.F., Shea, M.A., Tylka, A.J., Boberg, P.R.: 2006, A geomagnetic cutoff rigidity interpolation tool: accuracy verification and application to space weather. *Adv. Space Res.* **37**, 1206. DOI. ADS.

Stoker, P.H., Dorman, L.I., Clem, J.M.: 2000, Neutron monitor design improvements. *Space Sci. Rev.* **93**, 361. DOI. ADS.

Usoskin, I.G., Kovaltsov, G.A., Adriani, O., Barbarino, G.C., Bazilevskaya, G.A., et al.: 2015, Force-field parameterization of the galactic cosmic ray spectrum: validation for Forbush decreases. *Adv. Space Res.* **55**, 2940. DOI. ADS.

Usoskin, I.G., Gil, A., Kovaltsov, G.A., Mishev, A.L., Mikhailov, V.V.: 2017, Heliospheric modulation of cosmic rays during the neutron monitor era: calibration using PAMELA data for 2006 – 2010. *J. Geophys. Res.* **122**, 3875. DOI.

Vashenyuk, E.V., Balabin, Y.V., Perez-Peraza, J., Gallegos-Cruz, A., Miroshnichenko, L.I.: 2006, Some features of the sources of relativistic particles at the Sun in the solar cycles 21–23. *Adv. Space Res.* **38**, 411. DOI. ADS.

Villoresi, G., Dorman, L.I., Iucci, N., Ptitsyna, N.G.: 2000, Cosmic ray survey to Antarctica and coupling functions for neutron component near solar minimum (1996–1997): 1. Methodology and data quality assurance. *J. Geophys. Res.* **105**, 21025. DOI.

Vos, E.E., Potgieter, M.S.: 2015, New modeling of galactic proton modulation during the minimum of solar cycle 23/24. *Astrophys. J.* **815**, 119. DOI.

Woolf, R.S., Sinclair, L.E., Van Brabant, R.A., Harvey, B.J.A., Phlips, B.F., Hutcheson, A.L., Jackson, E.G.: 2019, Measurement of secondary cosmic-ray neutrons near the geomagnetic North Pole. *J. Environ. Radioact.* **198**, 189. DOI.